Tetraplex DNA Transitions within the Human c-*myc* Promoter Detected by Multivariate Curve Resolution of Fluorescence Resonance Energy Transfer†

Praveen Kumar,‡ Anjali Verma,‡ Souvik Maiti,‡ Raimundo Gargallo,§ and Shantanu Chowdhury*,‡

Institute of Genomics and Integrative Biology, CSIR, Mall Road, Delhi 110007, India, and Department of Analytical Chemistry, University of Barcelona, Marti i Franques 1-11, E-08028 Barcelona, Spain

Received July 25, 2005; Revised Manuscript Received September 28, 2005

ABSTRACT: The nuclease hypersensitive element (NHE) III_1 of the c-*myc* promoter regulates the expression of oncogene c-*myc* and hence is an important anti-cancer target. Paranemic secondary structure formation within the promoter has been implicated in mechanistic regulation models. Here, it is shown that two monomeric tetraplexes form within the c-*myc* promoter, which coexist in solution. The development and application of a new experimental approach for detection of conformation transitions in nucleic acids [which exploits the sensitivity of fluorescence resonance energy transfer (FRET) for theoretical spectral resolution by multivariate curve resolution-alternating least-squares (MCR-ALS) method] has been used for this study. The pK_a for tetraplex transitions are centered around 5.9 ± 0.2 (between two intercalation topologies) and 6.8 ± 0.1 (tetraplex to random coil). The presence of two tetraplexes has been further confirmed by S1 nuclease digestion. Finally, it is established that MCR-ALS analysis of FRET at different temperatures, pH, and salt concentrations allows resolution of pure species. Results are discussed in the light of recent observations implicating paranemic DNA motifs within the c-*myc* NHE in regulation of the oncogene. This method has several advantages over other methods vis-à-vis, high sensitivity and linear detection over a wide concentration range and, particularly, potential applications in intracellular probing.

DNA sequences with increased propensity to accumulate mutations and deletions or promote genome rearrangements have been classified as "at risk motifs" (ARMs) (*1*, *2*); a major proportion of such motifs are implicated in several human diseases (reviewed in ref *3*). Poly(dG/C)-rich sequences with a potential to form intramolecular four-stranded conformations are the most recent addition to ARMs (*4*). The poly-G form constitutes of a fold-back structure of stacked guanine tetrads held together by Hoogsteen hydrogen bonds (*5*), while pyrimidine (or C) tetraplexes are formed *in vitro* by poly-dC sequences. The latter were first identified by Gehring et al. and involve intercalated head-to-tail association of two duplexes stabilized by hemiprotonated C^+−C pairs in acid to neutral pH (*6*). Potential intrastrand C-tetraplex-forming elements have been identified within the centromeric human satellite III (*7*), telomeric fragment (*8*), and the nuclease hypersensitive element (NHE)[1] III_1 in the human c-*myc* promoter (*9*). The NHE is a major regulatory element of c-*myc*, wherein it has been postulated, on the basis of *in vitro* results, that expression is controlled by the binding of the transcription factor NM23-H2 preferably to the pyrimidine-rich sequence (*9*, *10*).

Several studies using NMR and X-ray crystallography have been undertaken to understand the structural characteristics of tetraplex motifs (*5*, *11*, *12*). The human telomeric DNA sequence $d[AG_3(T_2AG_3)_3]$ adopts a parallel tetraplex conformation, in the presence of K^+ ions, where the G repeats are oriented in the same direction and the loops are placed diagonally across (*13*, *14*). Interestingly, the same sequence adopts a completely different antiparallel motif in the presence of Na^+ ions (*12*). Different conformations were also observed within the G-quadruplex formed by c-*myc* NHE (*15*). Cytosine-rich sequence d(CCATTCCATTCCTTTCC) from the human centromeric satellite III forms two monomeric C-tetraplexes with different intercalation topology in response to pH (*7*). A natural sequence from the vertebrate telomere $d[(C_3TA_2)_3C_3T]$ was observed to fold intramolecularly at neutral pH and adopt at least two equilibrating conformations (*8*).

In addition to NMR and X-ray studies, fluorescence resonance energy transfer (FRET) has also been used to study tetraplex structures. Similar to molecular beacons, the fold-back structural motif in tetraplexes brings both ends of the sequence in proximity, making these structures interesting subjects for FRET. G-quadruplex formation *in vitro* by the G-rich NHE in the c-*myc* promoter (*16*) and C-tetraplex formation by a 21-mer cytosine-rich sequence from the vertebrate telomere were observed by FRET (*17*). Several recent reports use FRET of molecular beacons as intracellular probes (*18*−*20*). However, FRET has not been used to analyze conformation dynamics in nucleic acids.

In the context of the nucleic acid structure and conformation dynamics, multivariate curve resolution-alternating least

† This work was supported by research grants from DST, India (SERC FAST Track) to S.C., and Spanish MCyT (BQU2003-00191) to R.G.

* To whom correspondence should be addressed. Telephone: (91) 11-2766-7471. Fax: (91) 11-2766-7471. E-mail: shantanuc@igib.res.in.

‡ CSIR.

§ University of Barcelona.

[1] Abbreviations: MCR-ALS, multivariate curve resolution-alternating least squares; FRET, fluorescence resonance energy transfer; NHE, nuclease hypersensitive element.

10.1021/bi051452x CCC: $30.25
Published on Web 11/24/2005

squares (MCR-ALS) of UV and CD spectra has been used recently by Jaumot et al. to analyze the conformation transition between multiple coexisting species of a cyclic 8-mer oligonucleotide (*21*). It was also found useful for the resolution of protonation and denaturation equilibria of nucleic acids (*22*) and proteins (*23*). A recent paper by Duponchel et al. discusses the usefulness of multivariate resolution methods vis-à-vis other univariate methods and highlights its use in imaging spectroscopy (*24*).

In view of the advantages that FRET offers over methods such as NMR and X-ray crystallography with respect to intracellular probing, a method was recently developed for applying MCR-ALS on FRET spectra (*25*). Herein, this method has been applied to examine the *in vitro* conformation dynamics of the pyrimidine tetraplex formed in the c-*myc* NHE III_1. This is of interest in the context of c-*myc* activation for two primary reasons. First, the transcription factors hnRNP-K and NM23-H2, known to regulate c-*myc*, bind to the pyrimidine-rich strand in the promoter of c-*myc*. Thus, the observation that this strand adopts a structural motif may have a functional role in transcription factor binding (*9*, *26*). Second, in the context of the c-*myc* regulatory model implicating G-quadruplex formation within the NHE as a silencer element, the quadruplex/duplex conversion involving the complementary pyrimidine-rich strand is important (*27*). In this regard, the structural characteristics of the complementary strand is poorly understood. Results obtained here, using multivariate resolution of FRET spectra for the first time, show that multiple-folded pyrimidine tetraplexes are in equilibrium at neutral pH. This is discussed in light of altered binding interactions involving hnRNP-K and NM23-H2 and the duplex-binding affinity within the NHE (taken together with the G-quadruplex formed in the purine-rich strand) (*9*, *16*). Both of the factors have been postulated to be important in the regulation of c-*myc* (*27*).

MATERIALS AND METHODS

The 31-mer oligonucleotide d(CCC CAC CTT CCC CAC CCT CCC CAC CCT CCC C) from the promoter site of c-*myc* corresponding to bases 2281−2211 of the locus and the corresponding single-labeled (5′-fluorescein) and double-labeled [5′-fluorescein and 3′-tetramethylrhodamine (TAMRA)] oligonucleotide were obtained from Sigma Genosys. All reagents were of analytical grade. The single-strand oligonucleotide concentration was calculated according to Gray et al. using a molar extinction coefficient ($\epsilon_{260\ nm}$ = 7913 M^{-1} cm^{-1}) (*28*) for the labeled DNA sequences; $\epsilon_{260\ nm}$ values (fluorescein, 14 518; and TAMRA, 31 980 M^{-1} cm^{-1}) (*29*) were added for the respective oligonucleotides.

Circular Dichroism (CD) Spectroscopy. All CD measurements were performed on a Jasco Spectropolarimeter (model J 715) equipped with a thermostat-controlled cell holder with a cell path length of 1 cm as described previously (*26*). CD spectra were recorded from 220 to 400 nm with an averaging time of 3 s using 2.24 μM (or 16 μM) unlabeled oligonucleotide or 5′-fluorescein- and 3′-TAMRA-labeled oligonucleotide in 10 mM sodium cacodylate. pH titrations were performed at 20 °C by the addition of NaOH directly to 2 mL of 10 mM sodium cacodylate at pH 4.5 in a cuvette and monitoring pH using an Orion microelectrode, after allowing the solution to equilibrate for 30 min following the change of pH. Ionic titrations were done in 10 mM sodium cacodylate buffer at pH 5.3, 5.6, or 6.1 in 0, 20, 50, 70, or 100 mM sodium chloride at 20 °C. The cell-holding chamber was flushed with a constant stream of dry nitrogen to avoid water condensation on the surface of the cuvette.

S1 Nuclease Digestion and PAGE Using Fluorescent Oligonucleotide. Digestion was performed at two different pH: 7.0 and 5.3. Reaction mixtures contained 0.01 M Tris-HCl (pH 7.0) or 0.01 M sodium acetate (pH 5.3), 0.05 M NaCl, 1 mM $ZnCl_2$, and 5 units of S1 nuclease (US Biochemicals). The template, 5′-flourescein-labeled oligomer (6.5 μM in 15 μL of reaction mixture) was incubated overnight at 4 °C in respective buffers before initiating digestion at 37 °C by adding S1 nuclease and Zn^{2+}. Digestions were stopped by removing 5 μL aliqouts after 5 and 10 min, adding them to 4 μL of stop buffer (70% formamide and 57 mM EDTA at pH 7.5), and freezing. Frozen samples were added to loading buffer [blue dextran/formamide (1:4)] and heated at 95 °C for 1 min prior to loading on a 4.5% polyacrylamide gel and electrophoresed (90 min in 1× TBE running buffer) at 55 °C and 27 V/cm using the 3100 Genetic Analyzer (from Applied Biosystems). Fluorescent size markers were loaded along with the sample as internal standards. Bands were scanned by a CCD application integrated with the instrument.

FRET Experiments. For FRET experiments, 0.2 μM of the doubly labeled (5′-fluorescein and 3′-TAMRA) oligonucleotide in 10 mM sodium cacodylate buffer at pH 5.3, 5.6, or 6.1 was heated at 95 °C for 10 min and then slowly cooled to 4 °C before each experiment. Melting experiments in varying ionic strength were done with 0, 20, 50, 70, and 100 mM added sodium chloride at each pH. All experiments were performed using a Fluoromax 4 (Spex) spectrofluorimeter with an excitation and emission bandwidth of 2 and 5 nm, respectively, and a 0.2 × 1 cm micro-quartz cuvette. The excitation wavelength was set at 480 nm, although the absorption maximum of the donor is at 492 nm to minimize the acceptor absorption and emission spectra were recorded from 500 to 750 nm (*17*). The donor intensity at the acceptor emission wavelength (580 nm) was observed under identical conditions separately with an oligonucleotide labeled with fluorescein only and subtracted from the observed acceptor intensity to eliminate the contribution from the donor fluorescence. The proximity ratio, P, was calculated as $P = (I_A)/(I_A + I_D)$, where I_A and I_D are the intensities of the acceptor (580 nm) and donor (520 nm), respectively (*29*). The individual intensities were used instead of an integrated area around the emission peaks because this facilitates subtraction of the donor intensity (which was measured independently in analogous conditions using an identical oligonucleotide singly labeled with the donor fluorescein) after each measurement. Although P cannot be used to calculate the absolute distance between the fluorophores, like the FRET efficiency, it can be used in cases where only qualitative relative distance information is required because it is simpler to calculate (*29*). P was calculated as a function of the temperature to monitor tetraplex folding/unfolding.

Multivariate Analysis of CD and FRET Experiments. The whole set of CD spectra recorded along the acid−base titrations were analyzed using the hard-modeling procedure EQUISPEC (*30*), while data recorded for salt titrations were analyzed with the soft-modeling MCR procedure (*22*, *31*,

32) as described before (*25*). In brief, both procedures were applied to evaluate concentration profiles and pure spectra of spectroscopically active species present in the system from decomposition of experimental data matrix D according to the equation

$$D = CS^{T} + E \quad (1)$$

where C and S^T are respectively data matrixes containing concentration profiles and pure spectra for each one of these species or conformations present in the experiment. E contains residual noise not explained by the proposed species or conformations in C and S^T. Decomposition of matrix D is accompanied by mathematical ambiguities that affect the reliability of the resolved concentration and spectral profiles. These ambiguities are related to the presence of a relative low signal-to-noise ratio, the spectral selectivity (i.e., the existence of wavelengths where only one of the species absorbs), and the concentration selectivity (i.e., the existence of pH, salt, or temperature regions where only one of the species exists). Experimental data with a significant level of noise or showing poor spectral and/or concentration selectivity will be very difficult to solve. To overcome these difficulties, different approaches can be applied. One of them is constraining the calculated concentration profiles to fit a physicochemical model. In the case of CD data recorded along an acid−base titration, application of a hard-modeling method (EQUISPEC), which fits the concentration profiles to an acid−base model, was possible. In this case, decomposition of D is expected to be unambiguous. When analyzing data from salt titrations or melting experiments, the application of hard-modeling procedures was not possible, as those are still not developed for multivariate data analysis. In these cases, one way to overcome most of the above-commented ambiguities is the simultaneous analysis with MCR of several data matrixes corresponding to different experiments. Hence, FRET data recorded along several melting experiments were simultaneously analyzed as in eq 1 [for a more detailed explanation, see ref *31* and MCR webpage (www.ub.es/gesq/mcr/mcr.htm)]. The model used for MCR simultaneous analysis of several melting experiments at different pH and ionic strength is described by eq 2

$$\begin{bmatrix} D\ {}^{\text{pH5.30}}_{\text{0mM}} \\ D\ {}^{\text{pH5.30}}_{\text{20mM}} \\ \dots \\ D\ {}^{\text{pH6.10}}_{\text{100mM}} \end{bmatrix} = \begin{bmatrix} C\ {}^{\text{pH5.30}}_{\text{0mM}} \\ C\ {}^{\text{pH5.30}}_{\text{20mM}} \\ \dots \\ C\ {}^{\text{pH6.10}}_{\text{100mM}} \end{bmatrix} S^{T} + \begin{bmatrix} E\ {}^{\text{pH5.30}}_{\text{0mM}} \\ E\ {}^{\text{pH5.30}}_{\text{20mM}} \\ \dots \\ E\ {}^{\text{pH6.10}}_{\text{100mM}} \end{bmatrix} \quad (2)$$

A data pretreatment was made before the simultaneous analysis of matrices corresponding to different pH and ionic strength conditions, to remove most of the high variability of the FRET signal because of instrumental and experimental sources, which are usually also common to traditional molecular fluorescence techniques (*25*). Moreover, this inherent variability was even more dramatic because the whole set of FRET measurements was carried out along several weeks. First, the baseline drift for each experiment was removed. Second, the experimental spectra (rows of the matrix D) were individually normalized to Euclidean norm unity. No information concerning the relative concentrations of the different components formed in a melting experiment

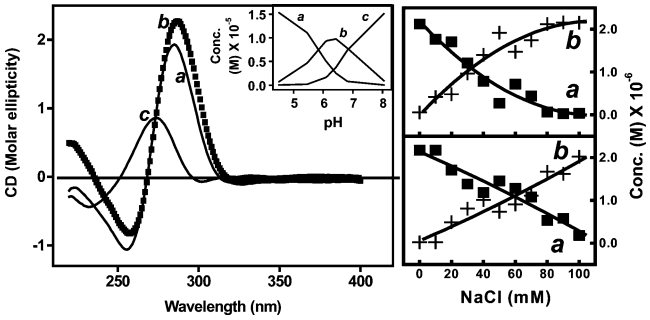

FIGURE 1: Evidence of two tetraplex conformations in solution. CD spectra were collected at various pH and NaCl concentrations and analyzed by multivariate resolution techniques as described in the Materials and Methods. pH was changed in the cuvette using NaOH and spectra of 16 μM oligonucleotide in 20 mM NaCl monitored after equilibrating for 30 min following each addition. (Left panel) a, b, and c show pure spectra as resolved by the multivariate analysis procedure EQUISPEC. The resolved concentration profiles, with respect to pH, for the three resolved species are shown in the inset (left panel). Panels on the right show MCR resolved concentration profiles and their dependence on sodium chloride concentration at pH 5.3 (top panel) and pH 5.6 (lower panel) with 2.24 μM oligonucleotide. a and b are respective tetraplex species as shown in the CD spectra. pH titration experiments were done in 10 mM sodium cacodylate at 20 °C. Concentration profiles for ionic titration experiments at 20 °C are shown.

or the shape of their concentration profiles is lost, because no normalization is carried out in the temperature direction (columns of the data matrixes) (*32*, *33*). A more detailed description on the advantages of the simultaneous analysis is given in ref *28*, *31*. All MCR calculations were performed using in-house MATLAB (version 6.5, The Mathworks Inc., Natick, MA) routines, which can be downloaded from the MCR webpage (ASCII files).

RESULTS

Conformation Changes in Tetraplexes Detected by Multivariate Analysis of CD Spectra. The cytosine-rich strand from the c-*myc* NHE has been observed to form an intramolecular C-tetraplex motif *in vitro* (*9*). Thermodynamics of folding of this motif was recently studied, and it was observed to be enthalpically driven and induced by the uptake of 2−3 mol of protons/mol of tetraplex (*26*). The monomeric nature of this fold-back motif was established under the experimental conditions used in this study by PAGE (Figure 3 of ref *26*) and concentration independence of melting profiles and electrophoresis bands (*26*). To further characterize the tetraplex structure under equilibrium conditions, the multivariate analysis procedure was used. This has been used for resolving of spectroscopic data to detect equilibrium conformers in nucleic acids in several studies (*21*, *22*, *34*). Figure 1 (left panel) shows resolved concentration profiles and pure CD spectra, analyzed from the acid−base titration monitored by CD, when EQUISPEC was applied. The presence of two C-tetraplexes, a and b, in the pH range 4.5−8.0 (inset) was evident from characteristic spectral positive (287 nm) and negative (256 nm) peaks for both the components, while species c observed at higher pH can be related to the unfolded single strand (*9*, *35*). An increased intensity of the positive peak along with a diminished intensity at the negative peak was observed for b. Interestingly, these characteristic features are indicative of a relatively higher participation of cytosine−cytosine$^+$ at neutral pH (*36*), which is surprising because hemi-protonation

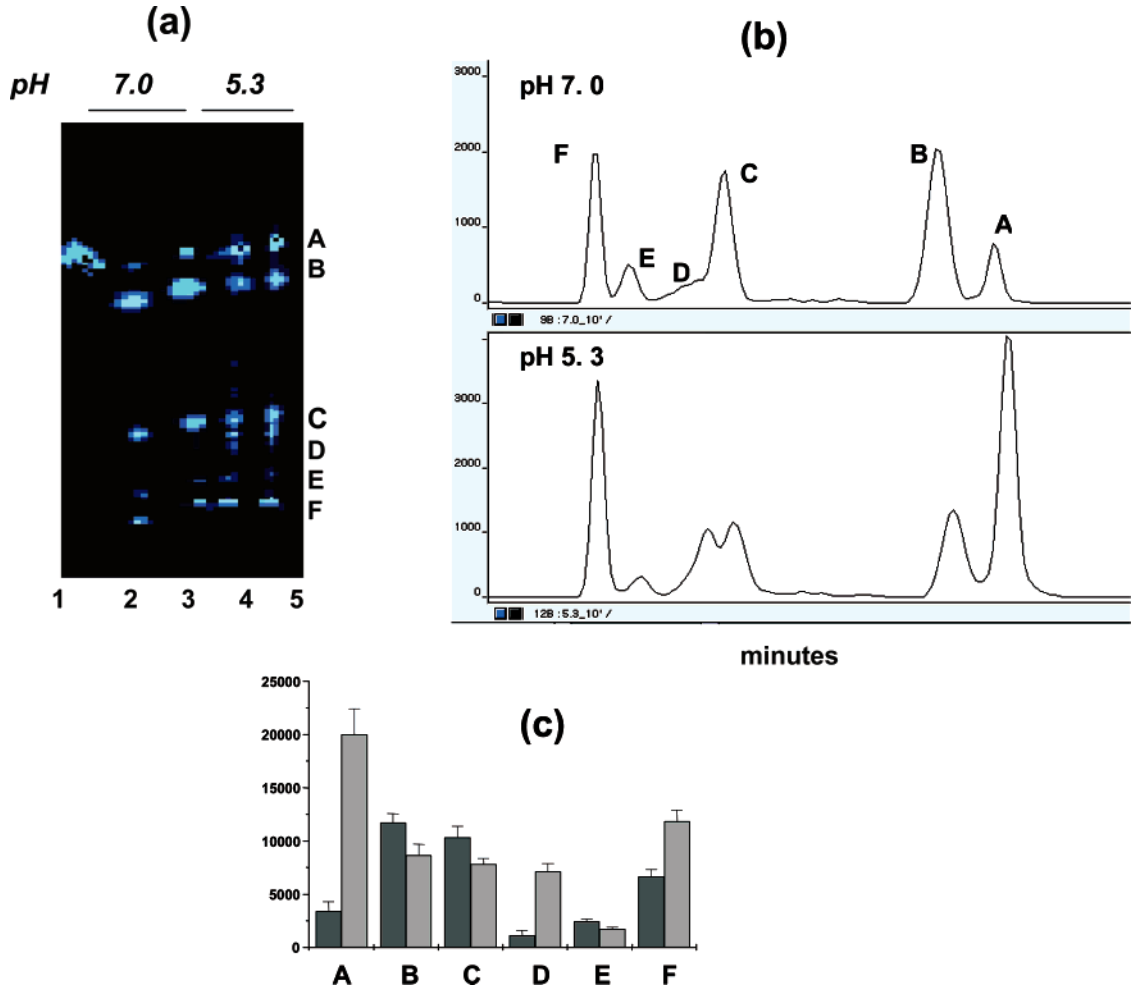

FIGURE 2: Two tetraplex conformations observed by S1 nuclease digestion. Denaturing gel electrophoresis was done following S1 nuclease digestion of the 5′-fluorescein-labeled 31-mer oligonucleotide at pH 5.3 and 7.0. The respective bands were monitored using a fluorescence detector. Band intensities were used to compare the cleavage pattern generated under the different conditions. (a) CCD image of fluorescent denaturing PAGE after S1 digestion. Untreated 31-mer sequence (lane 1); S1 treated at pH 7.0 for 5 min (lane 2) and 10 min (lane 3); and S1 treated at pH 5.3 for 5 min (lane 4) and 10 min (lane 5). The bands are labeled on the right margin. (b) Electrophoretogram showing cleavage profile at the indicated pH after 10 min of digestion; peak labels correspond to bands shown in a. Peak areas indicate the intensity of the fluorescent bands. (c) Bar graph comparing peak intensities of individual bands based on their respective peak area after 10 min of S1 treatment at pH 7 (dark bars) and pH 5.3 (light bars). A total of 6.5 μM oligonucleotide was digested in 0.01 M Tris-HCl (pH 7.0) or 0.01 M sodium acetate (pH 5.3), 0.05 M NaCl, 1 mM $ZnCl_2$, and 5 units of S1 nuclease at 37 °C and separated on a 4.5% polyacrylamide gel by electrophoresis at 55 °C and 27 V/cm using an Applied Biosystems 377 instrument. Values in bar graph are averaged from three independent experiments.

is expected to be favored at a lower pH. However, this may indicate that factors other than $C-C^+$ bonds in the core of the tetraplex may be responsible for stability. The estimated pH transition midpoints for the folded species were 5.9 ± 0.2 and 6.8 ± 0.1, both of which appear to be related to protonation of cytosine bases because adenine bases show protonation at pH values around 4 and thymine bases show deprotonation at pH values around 9 (*37*). The second pH midpoint agrees well with the one reported earlier (*9*, *26*), whereas the first transition has not been observed before. These results were confirmed by the soft-modeling multivariate analysis technique MCR (*22*, *31*, *32*) where the best results were obtained when three acid−base species were postulated. On considering only two acid−base species, high residuals were obtained at acidic pH, while no convergence was achieved when four species were considered (*25*). To ascertain that the resolved spectra were not artifacts of the analysis or the pH titration experiment, CD spectra of ionic strength titrations at different pH were also analyzed with MCR (right panels in Figure 1). Two tetraplexes could be observed at all of the pH values. The conformer predominant at higher ionic strength (species b) was the one with a higher number of $C-C^+$ bonds as indicated by their respective CD profiles [increased molar ellipticity at 287 nm (*36*, *38*)]. This appears to be consistent with the fact that a higher ionic strength has a destabilizing effect on i-motifs, in general, as observed in a previous study (*26*), and hence, more intercalated $C-C^+$ bonds may be required to withstand destabilization at increased ionic strength. Transition between the folded motifs was observed to occur between ~30−60 mM sodium ion concentration at all pH values studied.

S1 Nuclease Digestion Confirms Two Conformations. To distinguish between two putative C-tetraplex structures indicated by multivariate analysis of CD spectra, S1 nuclease digestion experiments were performed. Considering the dynamic equilibrium between the species, it was necessary to find digestion conditions such that cleavage patterns specific to predominant species could be distinguished. pH 5.3 and 7.0 were observed to give reasonably distinct cleavage patterns. Figure 2a shows the 5′-fluorescein-labeled

bands after S1 nuclease digestion, and Figure 2b shows the respective intensities of each band; the intensities are compared in bar graph based on their peak areas (Figure 2c). The cleavage pattern indicates that folded motifs with intervening single-nucleotide stretches are present at neutral pH, which is consistent with CD results and supports tetraplex formation. The evidence of folded C-tetraplex in this pH range has been reported before by CD and UV (*9*); however, nuclease digestion to confirm single-stranded loops in the proposed tetraplex was not done before. At pH 7.0, S1 nuclease induced three major cleavages showing the 5′-end-labeled bands B, C, and F (as marked on the right margin of the gel, Figure 2a) of about 24-, 16-, and 5-mer size (as indicated by size markers, with an error of ±1 base), respectively, and one minor band E (6-mer). All of the three major bands appear to be due to cleavage within the loops (the cleavage sites are indicated in the structural models shown in Figure 5 and discussed below). This is consistent with a tetraplex structure with eight $C-C^+$ base pairs (Figure 8 in ref *9*) proposed in a previous study. At pH 5.3, in addition to the presence of bands because of the structure predominant at neutral pH, band D was observed, which appears to be specific to the conformation at acidic pH (Figure 2c). As pointed out in Figure 5b, this band could result from cleavage within the two-nucleotide loop formed by a tetraplex with six $C-C^+$ bonds in the stem. A relatively higher amount of band F was also formed at pH 5.3, suggesting a cleavage within the overhang. It was clearly observed that the species at neutral pH was more S1-nuclease-sensitive than the one at a lower pH. The resistance of the folded state at a lower pH toward S1 nuclease cleavage is emphasized by the fact that S1 nuclease activity is optimal at a lower pH (4.0−4.3) and hence may indicate an intercalation topology with limited exposed single-strand segments.

Energy Transfer Because of Tetraplex Formation. To use FRET to detect the different conformations, energy transfer in the folded tetraplex was checked. FRET has been observed to be a sensitive method for the study of C-tetraplexes (*17*) and other nucleic acid structures (*39*). To observe FRET in the tetraplex, it was first established that the doubly labeled oligonucleotide required for FRET retained the tetraplex fold. The characteristic CD profile of a C-tetraplex was also given by the labeled oligonucleotide, although the intensity was somewhat lower, indicating that the fluorophores may be destablilizing the tetraplex (Figure 3a). Characteristic acceptor emission at 580 nm was observed at a low temperature, indicating energy transfer (Figure 3b). With increasing temperature, *P*, the fraction of the total observed fluorescence emitted by the acceptor, decreased, indicating a lowered energy transfer because of unfolding, which places donor and acceptor fluorophores beyond the critical Förster distance required for energy transfer (*17*). A plot of *P* versus temperature was analyzed for melting temperature T_M at pH 5.6 (inset). It is noteworthy that a sigmoidal melting transition curve was not observed, which could be due to a non-two-state transition equilibrium. Analogous trends were observed at pH 5.3 and 6.1 (data not shown). Table 1 lists T_M at each pH in 20 or 100 mM sodium ion concentration. The broad agreement in the melting temperatures measured by UV (*26*) and FRET indicated that the folding properties were largely retained after covalent attachment of fluorophores.

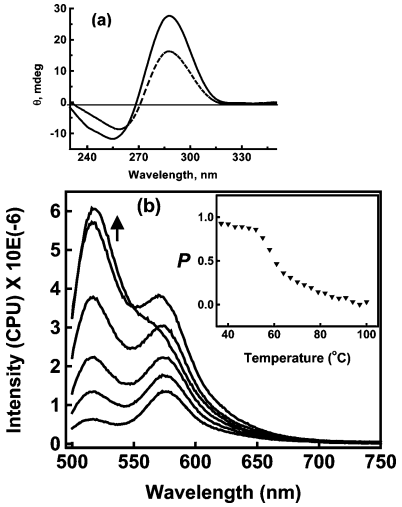

FIGURE 3: 31-mer cytosine-rich oligonucleotide folds into a tetraplex that shows FRET. Tetraplex conformation of the doubly labeled oligonucleotide was ascertained by CD and the loss in energy transfer because of thermal denaturation observed. (a) CD spectra of 2 μM unlabeled (—) or 5′-fluorescein and 3′-TAMRA doubly labeled (- - -) oligonucleotide at pH 6.5. (b) Fluorescence energy transfer of the labeled tetraplex. The arrow indicates a trend with increasing temperature (6, 22, 51, 57, 60, and 81 °C) at pH 5.60. The inset shows the proximity ratio *P*, calculated using the emission of the donor and acceptor (see the Materials and Methods), at pH 5.60 as a function of the temperature. All spectra were recorded with 0.2 μM oligonucleotide in 10 mM sodium cacodylate with 20 mM sodium chloride.

Table 1: Comparison of the Thermal Denaturation of the Oligonucleotide Monitored by UV Melting or FRET[a]

	pH 5.3		pH 5.6		pH 6.1	
	20 mM	100 mM	20 mM	100 mM	20 mM	100 mM
UV melting[b]	66.5	63.5	58.5	57.0	53.0	52.5
FRET[c]	67.5	60.0	56.5	53.5	51.0	50.0

[a] UV-melting experiments were done with unlabeled 31-mer oligonucleotide, and energy-transfer experiments were done with the 5′-fluorescein and 3′-TAMRA doubly labeled nucleotide at different pH and 20 or 100 mM sodium ion concentration. T_M values were determined from at least two replicates and are within 0.5 °C. [b] Determined from thermal denaturation observed at 260 nm (*35*). [c] Determined from the proximity ratio as observed in energy-transfer spectra versus temperature (see the Materials and Methods).

FRET Detects Conformation Dynamics of Tetraplexes. After the presence of two conformations was established by CD and S1 nuclease digestion and demonstrated that the folded motif showed energy transfer because of folding, FRET was used to detect the conformation exchange. FRET melting experiments (as shown in Figure 3) performed at different pH (5.3, 5.6, and 6.1) and various ionic strengths (0, 20, 50, 70, and 100 mM sodium chloride) were analyzed simultaneously after data pretreatment and normalization of raw spectra to Euclidean norm unity according to eq 2. The resolved pure FRET spectra are shown in Figure 4a. Emission (of TAMRA) at 580 nm in species a (pH 5.3) and b (pH 6.1) indicated energy transfer and could be attributed to folded structures, while the third spectra (species c) may be due to the unfolded state, which is consistent with CD results. Species a showed less energy transfer relative to species b, indicating a closer proximity of the 5′ and 3′ ends in the intercalated topology predominant at the higher pH. Parts b−d of Figure 4 show concentration profiles at pH 5.3, 5.6,

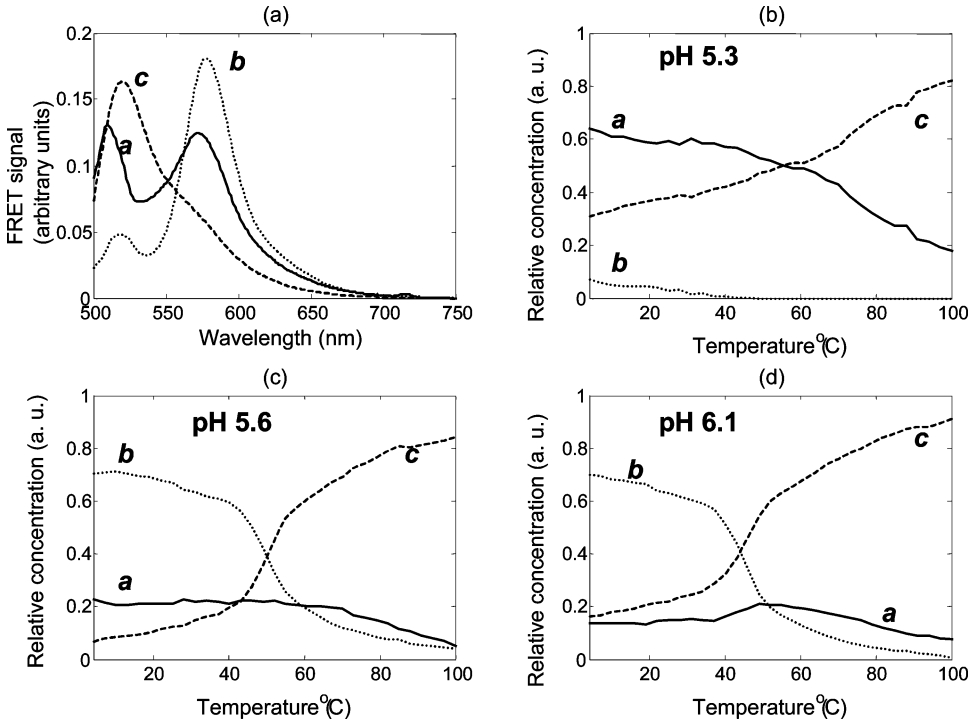

FIGURE 4: Two tetraplex conformations detected by FRET. Multivariate curve resolution (MCR) techniques were applied to experimentally observed energy-transfer spectra to resolve spectrum of single species and their concentration profiles as a function of the temperature as described in the Materials and Methods. (a) Resolved energy-transfer spectra obtained after simultaneous analysis by MCR. a, b, and c denote energy-transfer spectra because of respective conformations. (b, c, and d) MCR-generated concentration profiles on thermal denaturation in 50 mM NaCl at respective pH. Labels on respective conformations are as in a. (—) Ordered structure predominant at pH 5.3 (species a). (•••) Tetraplex predominant at pH 6.1 (species b). (- - -) Disordered conformation (species c). All experiments were done with 0.2 μM 5′-fluorescein and 3′ TAMRA doubly labeled oligonucleotide in 10 mM sodium cacodylate buffer at pH 5.3, 5.6, or 6.1 in 0, 20, 50, 70, or 100 mM sodium chloride.

and 6.1, respectively, in 50 mM sodium chloride as a function of temperature. The equilibrium at pH 5.3 was dominated by species a, while at pH 5.6 and 6.1, a marked shift in the concentration profiles of species in equilibrium was observed, with a very low presence of species a, indicating a transition of intercalation topology between pH 5.3 and 5.6. This was somewhat lower than that analyzed by CD (pH 5.9 for motif transition). The anomalous shift in the transition pH between the complimentary methods may be due to the difference in the experimental techniques used. Oligonucleotides employed to do FRET were doubly labeled with fluorophores, while the ones used for CD were unlabeled. Additionally, CD spectra were recorded after the establishment of equilibrium following each pH perturbation, while FRET spectra were recorded at one pH at a time.

The lack of fit was about 3.28% of the experimental data matrix *D*, which could be considered good, taking into account the instrumental technique and the large number of matrixes simultaneously analyzed, which were recorded under independent experimental conditions. In general, the concentration profiles were adequately resolved; however, the presence of species a at 100 °C (pH 5.3, Figure 4b) was anomalous. We believe that this arises primarily because of an experimental artifact associated with the FRET technique, wherein residual energy transfer is observed even at 100 °C when the doubly labeled oligonucleotide is expected to be fully unfolded. This may result because of some energy transfer in a random-coiled molecule, where the two fluorophores may be placed within Forster's distance. An additional reason could be poor resolution of spectral data in the melting experiments, which could be due to the high overlap between the concentration profiles of the three different components. It must be noted that the concentration of species a and b evolve in a similar way along the melting experiments, as observed in parts b−d of Figure 4. Moreover, the resolved pure FRET spectra show a strong overlap, without any selective wavelength. In these conditions, a complete mathematical resolution without any ambiguity, mainly for the minority species, is very difficult. However, it may be stressed that the results presented here are consistent with observed experimental data. A closer look at the resolved FRET spectra indicated that species a has a noticeable signal at 510 nm, which was not observed in species b. The shift in λ_{max} of fluorescein emission reinforces the point that the resolved spectra belong to different intercalation geometry and are not artifacts of the multivariate analysis procedure. The observed shift may be expected from a change in the microenvironment of fluorescein in the two structures, which could result from a variation in the proximity of the 5′ end from the tetraplex core. However, the possibility of an artifact generated from the experimental FRET observation cannot be ruled out. Nevertheless, the shapes of the spectra still signify a change in topology and hence are relevant to the conclusions made by us. In view of the fact that fluorescein emission is very sensitive to experimental conditions, such as pH, a variation in its emission might result from a different phenomenon than the intramolecular folding of the oligonucleotide (*17*). To address this concern, melting profiles of the 31-mer 5′-fluorescein-labeled oligonucleotide (without TAMRA at the 3′ end) were obtained at the three different pH values studied by us. After normalization of all of the melting profiles, it was concluded

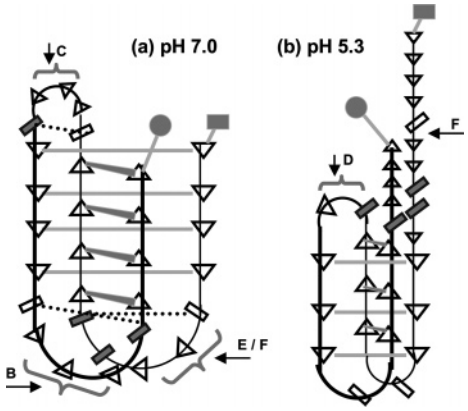

FIGURE 5: Schematic illustration of putative tetraplex conformations in pH-dependent equilibrium. Structural models are based on CD, S1 nuclease digestion, and FRET results observed in this study. Cytosine bases are represented as triangles pointed in the direction of strand polarity; empty rectangles are adenosines; and filled rectangles indicate thymines. Fluorescent labels are represented as gray box (fluorescein at the 5′ end) and gray circle (TAMRA at the 3′ end). (a) Tetraplex at pH 7.0 with a core of 8 $C-C^+$ base pairs; the dotted line shows the intraloop A·T pairs. (b) Tetraplex at pH 5.3 with a core of 6 $C-C^+$ base pairs. Arrows show the possible S1 nuclease sensitive sites, and arrow labels indicate bands observed in S1 nuclease digestion as marked in Figure 2.

that the observed variation in emission of fluorescein alone is rather small in comparison with the changes in the FRET signal produced because of unfolding of the ordered structure (*25*). Conclusions about the quantitative distance between the 5′ and 3′ ends based on energy transfer were not possible because the assumptions regarding isotropic distribution of fluorophores may not hold for folded and unfolded states as described in detail previously (*17*).

DISCUSSION

Thermodynamic characterization of the c-*myc* pyrimidine tetraplex based on univariate analysis was recently reported, where it was observed that the mobility of the band in native PAGE at pH 7.0 was different from pH 5.3 or 6.0, suggesting the presence of a differently folded species (*26*). On the basis of this, it was hypothesized that the pyrimidine tetraplex may be adopting multiple tetraplex motifs, which are in equilibrium. To explore this conformation transition, multivariate resolution was applied to energy-transfer spectra obtained from FRET (*25*).

On the basis of the results, models for the possible tetraplex conformations may be proposed (Figure 5). It is interesting to consider the characteristic stability of the tetraplex at neutral pH, where cytosine protonation is expected to be relatively weak. This may be due to the additional stabilization conferred by three Hoogsteen A·T base pairs (in the loop) stacked on the tetrad core (Figure 5a). A similar observation was made in the first high-definition structure obtained for the sequence d(5m$CCT_3CCT_3ACCT_3CC$), which has a well-defined C-tetraplex core with a Hoogsteen A·T pair in the loop, wherein this was considered as one of the factors conferring stability to the motif at neutral pH (*40*).

The major S1 nuclease cleavage bands obtained at neutral pH support this structure, where cleavage is observed only in the exposed loops (bands B, C, and F in Figure 5a). Consistent with this, CD results also indicate a topology involving a higher number of $C-C^+$ bonds at neutral pH (species b in Figure 1a). On the other hand, at pH 5.3, the A·T pairs would be disrupted because of adenine protonation (*7*), thus making a topology with eight $C-C^+$ and additional intraloop A·T pairs unfavorable. However, it must be noted that with an adenine pK_a of ~4 (*7*) the amount of protonated adenine expected at pH 5.3 may not be enough for sufficient structure disruption, unless the pK_a for adenine increases within the intercalated motif. Thus, additional factors or alternate structural possibilities cannot be ruled out.

At low pH, an alternative tetraplex conformation might be preferred involving tetrad geometry of six hemiprotonated cytosines (instead of eight), wherein the additional A·T-paired stability is not required. This may result in a topology at a lower pH with six hemiprotonated cytosines and short loops consisting of one or two nucleotides (Figure 5b), which would be consistent with the observed overall S1 nuclease insensitivity at low pH and relatively high amount of band D as shown in Figure 2c. The lower pH conformation leaves a 10- and 5-mer overhang at the 5′ and 3′ ends, respectively. However, bands because of digestion of these single-strand overhangs were not observed. There could be two possible reasons for this: (a) the overhangs are shielded from S1 nuclease by the bulk of the tetraplex moiety, and/or (b) at acidic pH, protonation of cytosines may assist mutual intercalation of the cytosine-rich overhangs into an intramolecular duplex, thereby resisting S1 nuclease digestion. Formation of intermolecular duplex at the ends can be ruled out because of concentration independence observed in melting experiments (*26*).

It is noteworthy that the results and the proposed model indicate a tetraplex moiety with a greater number of $C-C^+$ bonds at higher pH, which is interesting considering the fact that hemiprotonated cytosines are more stable at a lower pH. As detailed above, this may result because of destabilization of A·T base pairs at lower pH rendering the eight-cytosine core less stable. This is consistent with a recent study where the C-rich DNA fragment from human centromeric satellite III, d[$(CCATT)_2CCTTTCC$], was observed to have a pH-dependent equilibrium of two i-tetraplexes with a mid-titration point at pH 4.6 (*7*). It was proposed, on the basis of NMR, that the structure at higher pH was stabilized by intraloop A·T base pairing, which was disrupted under acidic conditions because of adenine protonation (*7*, *8*). Two intramolecular tetraplexes were also evident in the crystal structure of the sequence, d[$(CCCTAA)_3CCCT$] from vertebrate telomere, which were attributed to the orientation of the thymine and adenine residues in the loop (*8*). Finally, a previous study, using 22-, 27-, and 33-mer fragments from the c-*myc* NHE, proposed two types of intramolecular tetraplexes having six $C-C^+$ (for the 22- and 27-mer) or eight $C-C^+$ (formed by the 33-mer) in the core (Figure 8 in ref *9*). This was based on their UV−visible melting and CD results. It may be noted in this context that protonated cytosine residues have been observed at neutral pH in several triplex molecules, where cytosine was shown to have increased pK_a (*41*).

The proposed structural models agree with FRET results. The compact motif at neutral pH shows higher energy transfer because of close proximity of the two ends whereas at acidic pH the relative distance between the respective ends increases resulting in diminished energy transfer. Both the topological variations considered above with respect to the

end overhangs shown in Figure 5b (shielded overhangs or intercalated duplex formation) would be consistent with the diminished energy transfer observed. Multivariate analysis, applied for the first time on FRET data, allowed separation of the respective pure spectra from energy transfer recorded under equilibrium conditions. Simultaneous analysis of several spectral profiles, recorded along independent experiments, has been shown to be more powerful than separate individual analysis and allows improvement of the resolution of complex experimental data (*22*, *31*, *32*, *34*). In this study, spectroscopic FRET data recorded during experiments carried out in different experimental conditions were individually and simultaneously analyzed by multivariate curve resolution. The simultaneous analysis of several data matrixes allowed the resolution of the system, removing most of the ambiguities related to factor analysis. Detailed discussion of the application is presented elsewhere (*25*).

When the results obtained here are taken together, they help to establish the presence of topology variation as a result of pH and ionic strength changes in the c-*myc* C-tetraplex. It must be noted that the models are purely speculative and are proposed on the basis of inferences of results obtained in this study and indications in the literature. Clear explanations for these observations require detailed information of intercalation topology by NMR or X-ray crystallography.

There are certain drawbacks of using FRET that may be limiting factors at times. Typically, the purified yield of the doubly labeled oligonucleotide may be very low compared to the unmodified one and, more importantly, labeling may change the inherent characteristics of the oligonucleotide. Despite this, FRET is a preferred technique because of several advantages. It is very sensitive (can be detected at subnanomolar concentrations), allowing the use of a significantly low amount of oligonucleotide. Experiments can be followed across a wide concentration range (typically 4−5 orders of magnitude) because most spectrofluorimeters give a linear response over a wide range. Finally, FRET can be observed in the presence of other unlabeled molecules, making it an attractive technique vis-à-vis NMR for *in vivo* studies, particularly within cultured cells.

Biological Implications. Results obtained in this study, particularly the application of FRET together with multivariate analysis to observe conformation change, can be an advantage from several aspects. It can be used to study tetraplex-bound protein complexes in several proteins that have been characterized to bind to potential tetraplex-forming sequences *in vitro* (*42*−*45*). In the context of the particular sequence from the c-*myc* NHE studied here, the role of NHE in positive regulation of c-*myc* transcription has been established by several reports (*14*, *15*). It has been observed that a multifunctional protein nucleoside diphosphate kinase isoform B (NDPK-B) plays a major role in initiation of c-*myc* regulation (*46*, *47*) by binding preferably to pyrimidine-rich c-*myc* NHE (*10*). The heterogeneous nuclear ribonucleoprotein K (hnRNP-K), which activates c-*myc* expression, binds to the single-stranded pyrimidine-rich sequence within the NHE. Both of these factors may bind to the C-tetraplex form of NHE (*9*). The complementary G-rich strand also adopts the tetraplex motif (*16*). Siddiqui-Jain et al. recently observed the purine-rich motif to suppress c-*myc* expression (*27*). Stabilization (ligand-induced) of the motif led to a decrease in c-*myc* levels, while destabilization of the motif (by selective base substitution) increased c-*myc* levels. It has been further postulated that duplex−tetraplex switching in the NHE may be primarily responsible for regulation, and in this connection, it was recently observed that a single mutation within the NHE decreased the stability of the C-tetraplex and enhanced the potential of duplex formation (*48*). Collectively, these suggest a role of the tetraplex conformation(s) in regulation of c-*myc*; however, direct evidence of tetraplex binding to NDPK-B or hnRNP-K, *in vitro* or *in vivo*, is lacking. Observed results show that multivariate resolution of FRET may be used to elucidate the poorly understood role of tetraplex conformations in the transcription of c-*myc*.

ACKNOWLEDGMENT

S. M. and S. C. acknowledge Samir K. Brahmachari for constant support. P. K. and A. V. acknowledge research fellowships from CSIR. R. G. acknowledges a grant from the Spanish MCyT (BQU2003-00191). S. C. wishes to thank Ruma Banerjee, University of Nebraska−Lincoln, NE for carefully editing the manuscript. Authors thank Suruchika Soni and Arindam Maitra (The Centre for Genomic Applications, Delhi, India) for technical help in performing the PAGE experiments using 377 ABI sequencer.

REFERENCES

1. Gordenin, D. A., and Resnick, M. A. (1998) Yeast ARMs (DNA at-risk motifs) can reveal sources of genome instability, *Mutat. Res. 400*, 45−58.
2. Jinks-Robertson, S. (2002) The genome's best friend, *Nat. Genet. 31*, 331−332.
3. Bacolla, A., and Wells, R. D. (2004) Non-B DNA conformations, genomic rearrangements, and human disease, *J. Biol. Chem. 279*, 47411−47414.
4. Cheung, I., Schertzer, M., Rose, A., and Lansdorp, P. M. (2002) Disruption of dog-1 in *Caenorhabditis elegans* triggers deletions upstream of guanine-rich DNA, *Nat. Genet. 31*, 405−409.
5. Guschlbauer, W., Chantot, J. F., and Thiele, D. (1990) Four-stranded nucleic acid structures 25 years later: From guanosine gels to telomer DNA, *J. Biomol. Struct. Dyn. 8*, 491−511.
6. Gehring, K., Leroy, J. L., and Gueron, M. (1993) A tetrameric DNA structure with protonated cytosine−cytosine base pairs, *Nature 363*, 561−565.
7. Nonin-Lecomte, S., and Leroy, J. L. (2001) Structure of a C-rich strand fragment of the human centromeric satellite III: A pH-dependent intercalation topology, *J. Mol. Biol. 309*, 491−506.
8. Phan, A. T., Gueron, M., and Leroy, J. L. (2000) The solution structure and internal motions of a fragment of the cytidine-rich strand of the human telomere, *J. Mol. Biol. 299*, 123−144.
9. Simonsson, T., Pribylova, M., and Vorlickova, M. (2000) A nuclease hypersensitive element in the human c-*myc* promoter adopts several distinct i-tetraplex structures, *Biochem. Biophys. Res. Commun. 278*, 158−166.
10. Agou, F., Raveh, S., Mesnildrey, S., and Veron, M. (1999) Single strand DNA specificity analysis of human nucleoside diphosphate kinase B, *J. Biol. Chem. 274*, 19630−19638.
11. Balagurumoorthy, P., and Brahmachari, S. K. (1994) Structure and stability of human telomeric sequence, *J. Biol. Chem. 269*, 21858−21869.
12. Wang, Y., and Patel, D. J. (1993) Solution structure of the human telomeric repeat d[AG3(T2AG3)3] G-tetraplex, *Structure 1*, 263−282.
13. Parkinson, G. N., Lee, M. P., and Neidle, S. (2002) Crystal structure of parallel quadruplexes from human telomeric DNA, *Nature 417*, 876−880.
14. Neidle, S., and Parkinson, G. N. (2003) The structure of telomeric DNA, *Curr. Opin. Struct. Biol. 13*, 275−283.
15. Phan, A. T., Modi, Y. S., and Patel, D. J. (2004) Propeller-type parallel-stranded G-quadruplexes in the human c-*myc* promoter, *J. Am. Chem. Soc. 126*, 8710−8716.

16. Simonsson, T., Pecinka, P., and Kubista, M. (1998) DNA tetraplex formation in the control region of c-*myc*, *Nucleic Acids Res. 26*, 1167−1172.
17. Mergny, J. L. (1999) Fluorescence energy transfer as a probe for tetraplex formation: The i-motif, *Biochemistry 38*, 1573−1581.
18. Santangelo, P. J., Nix, B., Tsourkas, A., and Bao, G. (2004) Dual FRET molecular beacons for mRNA detection in living cells, *Nucleic Acids Res. 32*, E57.
19. Mitchell, P. (2001) Turning the spotlight on cellular imaging, *Nat. Biotechnol. 19*, 1013−1017.
20. Molenaar, C., Marras, S. A., Slats, J. C., Truffert, J. C., Lemaitre, M., Raap, A. K., Dirks, R. W., and Tanke, H. J. (2001) Linear 2′ *O*-methyl RNA probes for the visualization of RNA in living cells, *Nucleic Acids Res. 29*, E89.
21. Jaumot, J., Escaja, N., Gargallo, R., Gonzalez, C., Pedroso, E., and Tauler, R. (2002) Multivariate curve resolution: A powerful tool for the analysis of conformational transitions in nucleic acids, *Nucleic Acids Res*. *30*, E92.
22. Gargallo, R., Vives, M., Tauler, R., and Eritja, R. (2001) Protonation studies and multivariate curve resolution on oligodeoxynucleotides carrying the mutagenic base 2-aminopurine, *Biophys. J. 81*, 2886−2896.
23. Navea, S., de Juan, A., and Tauler, R. (2002) Detection and resolution of intermediate species in protein folding processes using fluorescence and circular dichroism spectroscopies and multivariate curve resolution, *Anal. Chem. 74*, 6031−6039.
24. Duponchel, L., Elmi-Rayaleh, W., Ruckebusch, C., and Huvenne, J. P. (2003) Multivariate curve resolution methods in imaging spectroscopy: Influence of extraction methods and instrumental perturbations, *J. Chem. Inf. Comput. Sci*. *43*, 2057−2067.
25. Kumar, P., Kajal, K., Gargallo, R., and Chowdhury, S. (2004) Application of multivariate curve resolution for the study of folding processes of DNA monitored by fluorescence resonance energy transfer, *Anal. Chim. Acta 536*, 135−143.
26. Mathur, V., Verma, A., Maiti, S., and Chowdhury, S. (2004) Thermodynamics of i-tetraplex formation in the nuclease hypersensitive element of human c-*myc* promoter, *Biochem. Biophys. Res. Commun. 320*, 1220−1227.
27. Siddiqui-Jain, A., Grand, C. L., Bearss, D. J., and Hurley, L. H. (2002) Direct evidence for a G-quadruplex in a promoter region and its targeting with a small molecule to repress c-*myc* transcription, *Proc. Natl. Acad. Sci. U.S.A. 99*, 11593−11598.
28. Gray, D. M., Hung, S. H., and Johnson, K. H. (1995) Absorption and circular dichroism spectroscopy of nucleic acid duplexes and triplexes, *Methods Enzymol. 246*, 19−34.
29. Green, J. J., Ying, L., Klenerman, D., and Balasubramanian, S. (2003) Kinetics of unfolding the human telomeric DNA quadruplex using a PNA trap, *J. Am. Chem. Soc. 125*, 3763−3767.
30. Dyson, R., Kaderli, S., Lawrence, G., Maeder, M., and Zuberbuhler, A. (1997) Second-order global analysis: The evaluation of series of spectrophotometric titrations for improved determination of equilibrium constants, *Anal. Chim. Acta 353*, 381−393.
31. Tauler, R., Smilde, A., and Kowalski, B. (1995) Selectivity, local rank, three-way data analysis, and ambiguity in multivariate curve resolution, *J. Chemom. 9*, 31−58.
32. Jaumot, J., Avino, A., Eritja, R., Tauler, R., and Gargallo, R. (2003) Resolution of parallel and antiparallel oligonucleotide triple helices formation and melting processes by multivariate curve resolution, *J. Biomol. Struct. Dyn. 21*, 267−278.
33. Jian-Hui, J., Yukihiro, O., Michael, K., and Heinz, W. S. (2004) Resolution of two-way data from on-line Fourier transform Raman spectroscopic monitoring of the anionic dispersion polymerization of styrene and 1,3-butadiene by parallel vector analysis (PVA) and window factor analysis (WFA), *Chemom. Intell. Lab. Syst. 70*, 83−92.
34. Gargallo, R., Tauler, R., and Izquierdo-Ridorsa, A. (1997) Application of a multivariate curve resolution procedure to the analysis of second-order melting data of synthetic and natural polynucleotides, *Anal. Chem. 69*, 1785−1792.
35. Manzini, G., Yathindra, N., and Xodo, L. E. (1994) Evidence for intramolecularly folded i-DNA structures in biologically relevant CCC-repeat sequences, *Nucleic Acids Res. 22*, 4634−4640.
36. Antao, V. P., and Gray, D. M. (1993) CD spectral comparisons of the acid-induced structures of poly[d(A)], poly[r(A)], poly-[d(C)], and poly[r(C)], *J. Biomol. Struct. Dyn. 10*, 819−839.
37. Izatt, R. M., Christensen, J. J., and Rytting, J. H. (1971) Sites and thermodynamic quantities associated with proton and metal ion interaction with ribonucleic acid, deoxyribonucleic acid, and their constituent bases, nucleosides, and nucleotides, *Chem. Rev. 71*, 439−481.
38. Cantor, C. R., Warshaw, M. M., and Shapiro, H. (1970) Oligonucleotide interactions. 3. Circular dichroism studies of the conformation of deoxyoligonucleotides, *Biopolymers 9*, 1059−1077.
39. Gelfand, C. A., Plum, G. E., Mielewczyk, S., Remeta, D. P., and Breslauer, K. J. (1999) A quantitative method for evaluating the stabilities of nucleic acids, *Proc. Natl. Acad. Sci. U.S.A. 96*, 6113−6118.
40. Han, X., Leroy, J. L., and Gueron, M. (1998) An intramolecular i-motif: The solution structure and base-pair opening kinetics of d(5mCCT3CCT3ACCT3CC), *J. Mol. Biol. 278*, 949−965.
41. Leitner, D., Schroder, W., and Weisz, K. (2000) Influence of sequence-dependent cytosine protonation and methylation on DNA triplex stability, *Biochemistry 39*, 5886−5892.
42. Lacroix, L., Lienard, H., Labourier, E., Djavaheri-Mergny, M., Lacoste, J., Leffers, H., Tazi, J., Helene, C., and Mergny, J. L. (2000) Identification of two human nuclear proteins that recognise the cytosine-rich strand of human telomeres *in vitro*, *Nucleic Acids Res. 28*, 1564−1575.
43. Marsich, E., Xodo, L. E., and Manzini, G. (1998) Widespread presence in mammals and high binding specificity of a nuclear protein that recognises the single-stranded telomeric motif (CCCTAA)n, *Eur. J. Biochem. 258*, 93−99.
44. Sarig, G., Weisman-Shomer, P., Erlitzki, R., and Fry, M. (1997) Purification and characterization of qTBP42, a new single-stranded and quadruplex telomeric DNA-binding protein from rat hepatocytes, *J. Biol. Chem. 272*, 4474−4482.
45. Eid, J. E., and Sollner-Webb, B. (1995) ST-1, a 39-kDa protein in *Trypanosoma brucei*, exhibits a dual affinity for the duplex form of the 29-base-pair subtelomeric repeat and its C-rich strand, *Mol. Cell Biol. 15*, 389−397.
46. Postel, E. H., Berberich, S. J., Flint, S. J., and Ferrone, C. A. (1993) Human c-*myc* transcription factor PuF identified as nm23-H2 nucleoside diphosphate kinase, a candidate suppressor of tumor metastasis, *Science 261*, 478−480.
47. Berberich, S. J., and Postel, E. H. (1995) PuF/NM23-H2/NDPK-B transactivates a human c-*myc* promoter-CAT gene via a functional nuclease hypersensitive element, *Oncogene 10*, 2343−2347.
48. Halder, K., Mathur, V., Chugh, D., Verma, A., and Chowdhury, S. (2005) Quadruplex−duplex competition in the nuclease hypersensitive element of human c-*myc* promoter: C to T mutation in C-rich strand enhances duplex association, *Biochem. Biophys. Res. Commun. 327*, 49−56.

BI051452X